International Forum on Aeroelasticity and Structural Dynamics
IFASD 2026
17-21 June 2026, Goettingen, Germany

# GROUND EXPERIMENTAL TESTS AND FLIGHT TEST DESIGN FOR A FLEXIBLE AIRCRAFT FLYING DEMONSTRATOR

**Pedro J. González**[1], **Guilherme C. Barbosa**[1], **Álvaro A. G. Quesada**[1], **Gerrit Stavorinus**[1], **Flávio J. Silvestre**[1], **Wolf R. Krüger**[2]

[1]Technical University of Berlin
Marchstraße 12, 10587 Berlin, Germany
p.gonzalez.ramirez@tu-berlin.de
g.chaves.barbosa@tu-berlin.de
garcia.quesada@campus.tu-berlin.de
gerrit.s.stavorinus@campus.tu-berlin.de
flavio.silvestre@tu-berlin.de

[2]DLR, German Aerospace Center,
Bunsenstraße 10, 37073 Goettingen, Germany
Wolf.Krueger@dlr.de

**Keywords:** High Aspect Ratio, Flexible Aircraft, Ground Tests and Flight Test Simulation

**Abstract:** This work presents the development and experimental validation of a structured, bottom-up approach for airworthiness assessment and flight-test preparation of the flexible aircraft demonstrator, TU-Flex. The proposed methodology extends the experimental validation block within the overall design workflow by incorporating full-aircraft characterization and ground testing to provide consistent feedback for model updating. The approach integrates center of gravity and inertia measurements, full-aircraft ground vibration testing, system integration checks, and progressive ground maneuverability and taxiing tests. These activities enable the identification of the aircraft mass and structural dynamic properties, the verification of system functionality, and the assessment of operational readiness prior to flight. The resulting data are used to update a flexible aircraft model implemented in a simulation testing environment, which supports the definition of flight-test maneuvers and pilot training. The experimental results show good agreement between measured and predicted structural dynamics, while highlighting the importance of experimental characterization of inertia properties. Ground tests confirm stable communication links, adequate controllability, and reliable system performance. The first flight test demonstrates safe takeoff, stable flight behavior, and consistent aeroelastic response, with observed structural deformations remaining within the expected range. The proposed framework provides a systematic connection between ground testing, model validation, and flight-test preparation, supporting the use of the TU-Flex platform as a representative flexible aircraft demonstrator for future aeroelastic, flight dynamics, and flight control studies.

## 1 INTRODUCTION AND MOTIVATION

High Aspect Ratio Wing Aircraft (HARW) design poses unique challenges due to the coupling between flight-dynamics and structural-dynamics modes. The increase in aspect ratio has a direct influence on the reduction of fuel consumption and carbon emissions due to the increase in aerodynamic efficiency. As a consequence of this increase in span, the aircraft wing becomes more flexible, and its structural dynamics modes decrease in frequency, starting to interact with the flight dynamics modes. This interaction deteriorates the flight control system performance and the aircraft's flying qualities. Therefore, the conventional approach of studying aeroelasticity and flight dynamics separately is no longer valid, and integrated models of flexible aircraft are necessary [1].

In this context, experimental investigations become essential to better understand and validate the coupled behavior between flight dynamics and structural dynamics in flexible aircraft. In particular, the development of dedicated flying platforms allows the acquisition of representative flight data under controlled conditions, enabling the assessment of integrated modeling approaches and their limitations [2].

The TU-Flex concept has been developed as a modular flying platform to explore the flight dynamics of flexible transport aircraft configurations [3]. The main objective of this platform is to complete flight experiments to collect coupled motion between flight and aeroelastic dynamics in response to control inputs. Two versions of the demonstrator have been built: the TU-Flex FW (Flexible Wing), representing the baseline flexible configuration, and the TU-Flex FW-P (Flexible Wing with Pod), which incorporates additional tip masses on the wings. These pods reduce the structural frequencies of the wing, increasing the coupling between wing flexibility and aircraft flight dynamics, thereby simulating the behavior of a very flexible aircraft while retaining the same wing structure. This approach enables a progressive validation of aeroelastic and flight dynamic models, from moderate to higher structural dynamic complexity [3–6].

The main distinction in the conceptual design of this vehicle, in comparison with conventional industrial processes, lies in the consideration of structural flexibility from the early design stages. Then, for the demonstration of a certain level of structural flexibility, it needs to be specified a priori. Once the design requirements are defined, the process enables the evaluation of different aircraft configurations and design decisions, as well as their influence on the structural and flight dynamics of the complete vehicle. The design process of the TU-Flex demonstrator is oriented toward promoting coupling between structural and flight-dynamics modes while increasing wing deformation. To this end, an iterative approach has been established, integrating different tools and frameworks to facilitate and accelerate the design process. The objective is to define a workflow in which modifications to the structure, geometry, or materials can be efficiently assessed, allowing the evaluation of their impact on the overall flight dynamics of the flexible vehicle. The final design is intended to represent the challenges associated with HARW aircraft and configurations with long, slender wings, characterized by large deformations and low structural frequencies interacting with rigid-body motion. The proposed iterative design process is presented in Fig. 1.

The conceptual design block defines the overall aircraft configuration based on initial requirements, integrating weight estimation, aerodynamic definition, structural layout, and stability considerations within an iterative workflow. Starting from statistical weight approximations and flight envelope constraints, the geometry of the wing, tail, and control surfaces is progressively refined through aerodynamic analyses and stability assessments. Airfoil selection and planform definition are driven by low-Reynolds-number performance, while stability and handling qualities are ensured through coupling with flight dynamics tools. A preliminary structural layout is incorporated early in the process using simplified models, allowing the evaluation of deformation levels and their interaction with flight dynamics. The process iterates until a feasible configuration is obtained that satisfies aerodynamic performance, structural flexibility, and flight dynamics requirements [3].

The aeroelastic optimization block focuses on the design of the flexible wing, aiming to maximize deformation and enhance coupling between structural and flight-dynamics modes while satisfying structural constraints. The wing architecture, including control surface layout, internal structure, and material distribution, is defined to accommodate both instrumentation and actuation systems. A coupled toolchain integrating finite element modeling, aerodynamic analysis, and optimization algorithms is used to evaluate structural responses and sensitivities. The optimization process considers laminate thicknesses, material orientations, and structural layouts as design variables, with constraints on strain and operational load cases. Multiple configurations are assessed iteratively, balancing wing mass, deformation, and manufacturability. The resulting design provides a structurally feasible and highly flexible wing, suitable for representing the targeted aeroelastic behavior of HARW configurations, following the methodologies presented in [2,4,5].

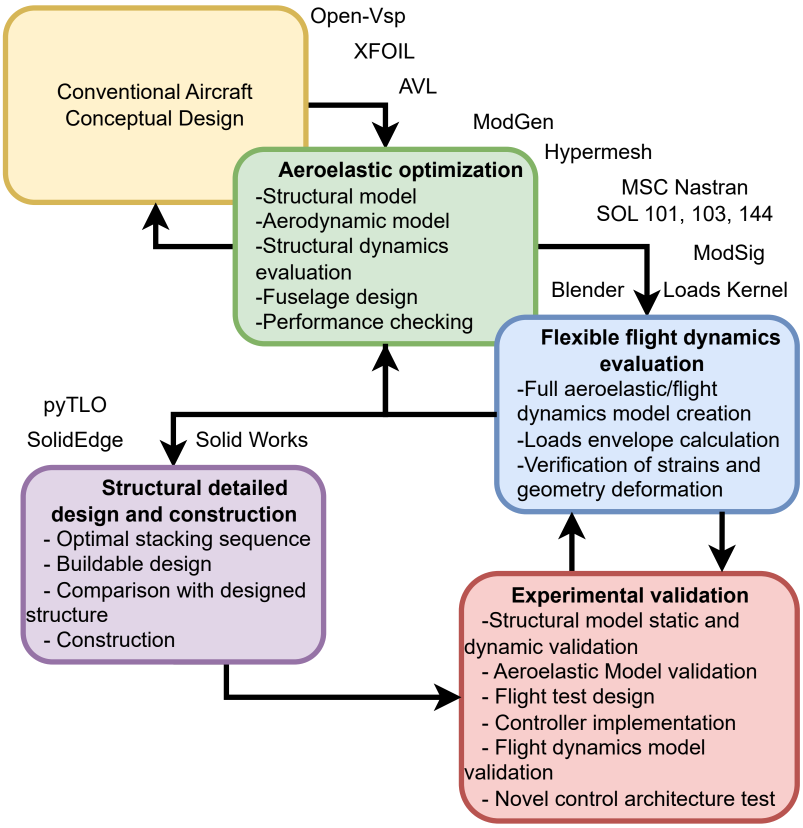


Figure 1: Flying demonstrator design workflow.

The flexible aircraft flight dynamics model and loads evaluation block provides an integrated framework for assessing both the aeroelastic behavior and structural integrity of the complete aircraft configuration. It is coupled with the aeroelastic optimization, detailed design, and experimental validation blocks, and supports the design of static, dynamic, and flight test campaigns. The Loads Kernel branch is used to evaluate structural loads across the flight envelope by coupling aerodynamic and structural models, enabling the computation of trim conditions, maneuver loads, gust responses, and landing scenarios. It provides nodal and sectional loads, which are used to generate load envelopes for structural verification [7,8]. In parallel, the Mod-

SiG branch enables nonlinear and linear flight dynamics simulations of the flexible aircraft, based on a modal representation of the structure combined with aerodynamic models based on strip theory. This framework captures the coupling between rigid-body motion and structural deformation, including unsteady aerodynamic, stall and follower forces effects and control inputs, and provides both time-domain responses and stability analyses [9–11]. Together, both branches allow verification of load-carrying capability and assessment of the intended aeroelastic coupling prior to progressing to detailed design.

The detailed design and construction block translates the optimized structural concepts into manufacturable components, ensuring that the final aircraft meets the targeted mechanical and aeroelastic properties. The outputs of the structural optimization are first converted into realistic composite stack-up sequences using the pyTLO framework, which applies genetic algorithms to determine feasible laminate configurations that satisfy both performance and manufacturing constraints [12]. The resulting designs are validated through finite element analyses to ensure consistency with the original structural and dynamic behavior. Subsequently, detailed CAD models are generated and used to produce molds for manufacturing. The aircraft components are fabricated using composite layup techniques, with material selection tailored to structural and functional requirements, combining glass and carbon fiber elements. The construction process includes manual layup, vacuum-assisted curing, and assembly of all structural components. This block ensures that the designed aeroelastic characteristics are preserved in the physical aircraft while maintaining manufacturability and structural reliability.

The experimental validation block is designed to generate high-quality data for model validation and control system development through a bottom-up testing approach. It begins with structural validation of the wing as a clamped system, including static loading and ground vibration testing to characterize deformation, natural frequencies, and mode shapes, and to calibrate the structural models [6]. These tests are complemented by aeroelastic validation in the wind tunnel, where the wing is evaluated under representative flow conditions to capture both steady and unsteady aerodynamic responses, as well as the effects of control surface actuation. The integration of onboard sensors and external measurement systems enables the collection of comprehensive datasets for validating aerodynamic and aeroelastic models. Finally, the flight test campaign is conducted in successive phases, starting with operational verification, followed by system identification maneuvers for tuning the flight dynamics model, and concluding with closed-loop experiments to assess advanced control strategies. This progressive validation strategy ensures consistency between numerical models and experimental results, while enabling the TU-Flex platform to support the study of coupled flight dynamics and aeroelastic behavior. So far, the experimental validation work has supported the collection of data for structural dynamics and aeroelastic model validation of the wings [13]. Limited work has been conducted on fully integrated flexible aircraft systems. Therefore, before initiating the flight test campaign associated with the experimental validation block, it is necessary to establish a comprehensive framework that combines full-aircraft ground testing and simulated flight test campaigns to ensure the safe operation of the demonstrator.

The main objective of this research is to define, implement, and experimentally validate a structured, bottom-up approach for airworthiness assessment and flight test preparation of a flexible aircraft demonstrator. This approach aims to ensure that the updated structural, aeroelastic, and inertial models accurately represent the full-vehicle dynamics prior to system identification campaigns. The TU-Flex demonstrator has been fully assembled, including its primary structure, modular wing components, and integrated electric propulsion and avionics systems, as shown in Fig. 2. Before proceeding to flight testing, a comprehensive series of ground tests and evaluations is conducted to assess the airworthiness of the aircraft with a flexible wing configuration.

Figure 2: TU-Flex with flexible wings.

## 2 EXPANSION OF THE EXPERIMENTAL VALIDATION BLOCK FOR THE COMPLETE AIRCRAFT

The primary objective of the TU-Flex demonstrator is to obtain experimental data to support both model validation and the development of advanced control strategies for flexible aircraft. For this purpose, it is crucial to ensure that the data collected during flight testing is of high quality and that the corresponding models are properly calibrated. The bottom-up validation strategy adopted for TU-Flex is presented in Fig. 3.

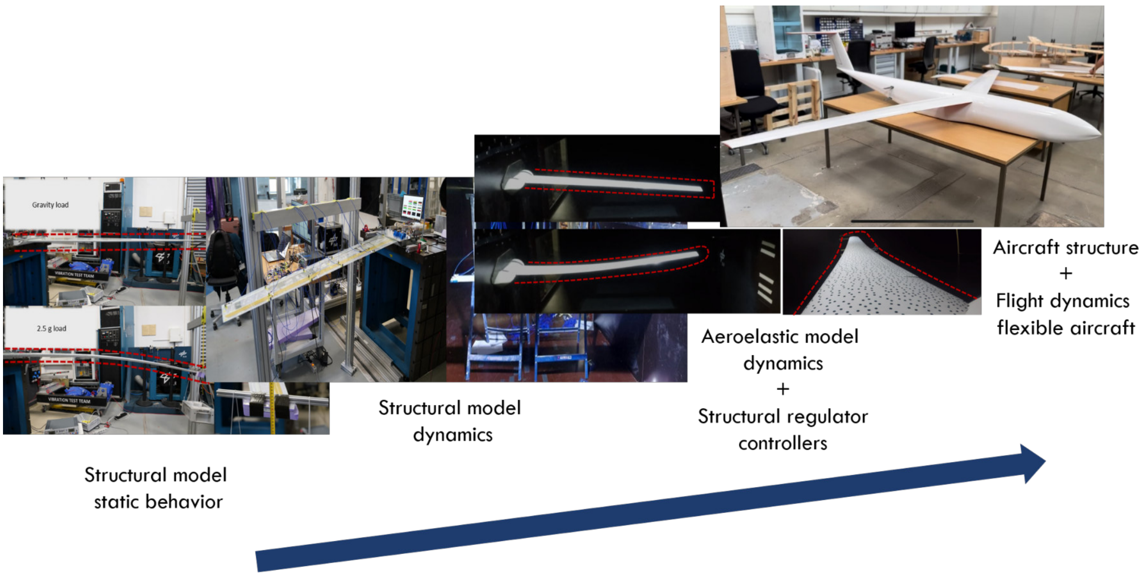


Figure 3: Bottom to top TU-Flex experimental validation approach.

This methodology starts with the assessment of the wing as a clamped structure. The validation campaign for the structural, dynamic, and aeroelastic models of the wing is divided into three main phases: static loading tests, ground vibration testing, and wind tunnel experiments [6]. Owing to the modular design of the aircraft, the wing can be readily installed on rigid test setups and wind tunnel balances, allowing dedicated investigations of its structural and aeroelastic characteristics. The expanded experimental validation block then introduces the full aircraft into the validation process. After full integration, including all sensors and onboard systems, the position of the center of gravity must be assessed and adjusted within operational limits, and the inertia properties must be measured. In addition, a ground vibration test of the complete integrated structure is required to update the flight dynamics model and support the design of the flight test campaign. At this stage, the experimental validation block feeds back updated information to the flexible aircraft evaluation block, enabling simulation-based assessment of the aircraft behavior. Subsequently, a ground test campaign is conducted to evaluate the readiness of the platform for field operation, including checks for electromagnetic interference, communication issues, and overall system performance. The aircraft performance on the ground is also assessed during these tests. The expanded experimental validation block is presented in Fig. 4. Once all these evaluations are completed, the flight test campaign can be carried out to acquire data for validating the flight dynamics model and for evaluating control approaches for flexible configuration.

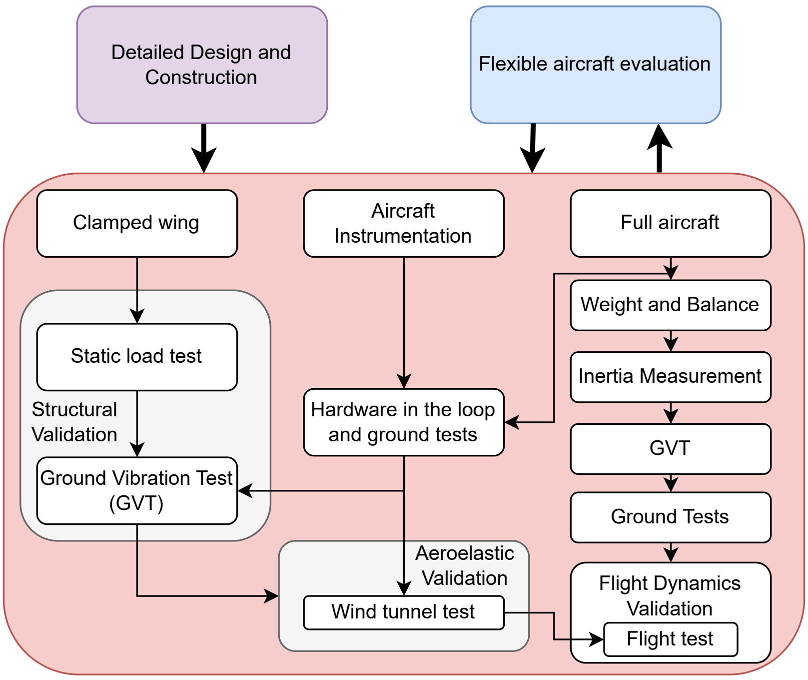


Figure 4: Experimental validation block diagram.

## 3 CENTER OF GRAVITY AND INERTIA MEASUREMENTS

The position of the Center of Gravity (CG) is critical to ensure the static stability of the aircraft, as well as to enable proper rotation during takeoff. Therefore, prior to each flight, the CG position is measured along the $x$ and $y$ axes using the datum method. In this approach, a fixed imaginary vertical plane is defined at the nose of the aircraft, from which all horizontal distances (arms) are measured for weight and balance calculations. The aircraft, with the landing gear extended, is placed on three balances, and the load on each wheel is measured. This procedure is repeated three times to reduce measurement uncertainty. The maximum takeoff weight of the aircraft is 24.99 kg, and the CG limits are defined between $X_{CG_{min}} = 0.11\bar{c}$ and $X_{CG_{max}} = 0.37\bar{c}$, (corresponding to static margins of 26% and 0%, respectively) measured from the leading edge of the wing. The $z$-component of the CG is obtained from the updated CAD model.

Measuring the inertia properties of an aircraft is essential for accurately predicting its dynamic behavior and stability characteristics. The mass distribution directly influences the equations of motion, affecting the response to control inputs, disturbance rejection, and overall flight performance. Therefore, reliable inertia estimation is a key requirement for flight dynamics modeling, simulation, and control system design [14]. In this work, a pendulum method is applied, in which the moments of inertia are determined from the oscillatory behavior of the aircraft when suspended about a given axis [15].

The pendulum method setup is presented in Fig. 5. The aircraft is mounted on a suspension system and allowed to oscillate about the axis of interest, while the corresponding periods are measured. The inertia is obtained by comparing the dynamic response of the combined system (aircraft plus rig) with that of the rig alone, allowing the isolation of the aircraft contribution.

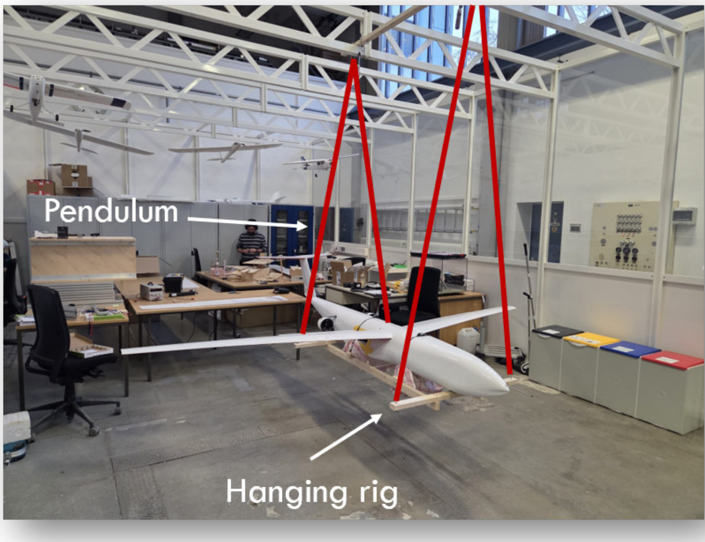


Figure 5: Inertia measurement using the pendulum method.

For the roll and pitch axes, the moments of inertia are calculated using

$$I_x = \frac{W_1 T_1^2 L_1}{4\pi^2} - \frac{W_2 T_2^2 L_2}{4\pi^2} - \frac{W_3 L_3^2}{g} \tag{1}$$

$$I_y = \frac{W_1 T_1^2 L_1}{4\pi^2} - \frac{W_2 T_2^2 L_2}{4\pi^2} - \frac{W_3 L_3^2}{g} \tag{2}$$

where $W_1$ is the weight of the aircraft and rig, $W_2$ the weight of the rig, and $W_3$ the weight of the aircraft. The parameters $L_1$, $L_2$, and $L_3$ represent the distances from the pivot point to the center of gravity of the combined system, the rig, and the aircraft, respectively, while $T_1$ and $T_2$ correspond to the measured oscillation periods.

For the yaw axis, a bifilar pendulum configuration is used, and the moment of inertia is obtained from

$$I_z = \frac{W_1 T_1^2 A^2}{16\pi^2 L} - \frac{W_2 T_2^2 A^2}{16\pi^2 L} \quad (3)$$

where $L$ is the length of the suspension fibers and $A$ is the distance between them. This formulation allows the isolation of the aircraft inertia by subtracting the contribution of the supporting rig. All equations are taken from [15], and repeated measurements are performed to reduce uncertainty and improve the accuracy of the identified inertia components.

## 4 FULL AIRCRAFT GROUND VIBRATION TESTING

The Ground Vibration Test (GVT) was conducted to identify the natural frequencies and mode shapes of the complete aircraft structure. This information is essential for tuning the flexible aircraft flight dynamics model. The test cases were designed to capture the dynamic behavior of the main structural components of the aircraft, including the wings, empennage, and fuselage.

To perform the test, a Siemens SCADAS data acquisition system was used, equipped with 15 uniaxial accelerometers, an instrumented excitation hammer, and Simcenter Testlab software for modal analysis. Prior to testing, the FEM model was used to predict the vibration modes and frequencies. Since the primary purpose of this model is to represent the structural dynamics within the flexible aircraft model, the frequency range of interest was limited to 40 Hz. Based on these predictions, two sensor configurations were defined to capture the dynamic response of the aircraft.

The sensor layout was designed to distribute the accelerometers along the wings, tail, and fuselage. The first configuration focuses on capturing vertical motion, while the second configuration targets in-plane modes of the wings and horizontal stabilizer, as well as lateral motion of the vertical stabilizer and fuselage. In the first setup, the sensors were placed along the front spar of the lifting surfaces and along the fuselage centerline. In the second setup, the sensors were mounted using 3D-printed adapters located at the leading edge of the wings and horizontal stabilizer, and on the main spar of the vertical stabilizer. Both setups are shown in Fig. 6.

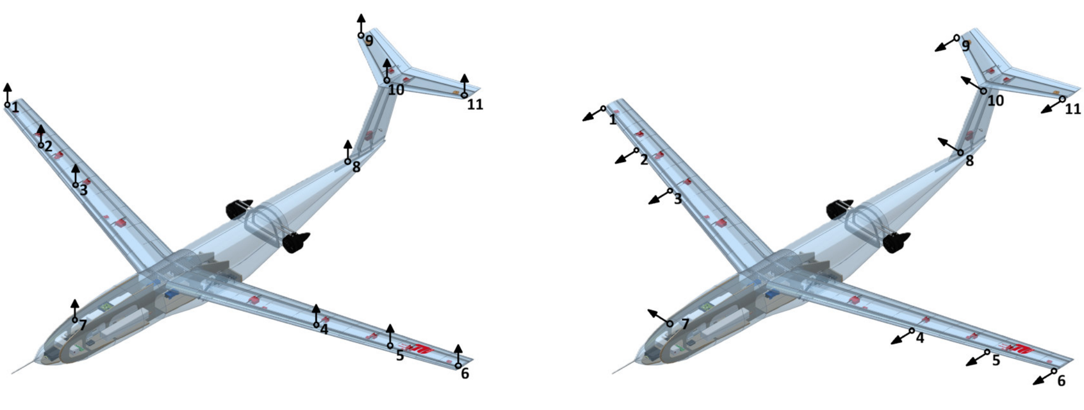


Figure 6: GVT out-of-plane sensor distribution (left). GVT in-plane sensor distribution (right).

During the GVT, the structure was excited at multiple locations. For out-of-plane excitation, impacts were applied at the mid-span and wingtip of the left wing, as well as at the horizontal stabilizer. For in-plane excitation, two impact points were considered: one at the wingtip and another at the tip of the horizontal stabilizer.

To identify the structural dynamics of the aircraft under free-flight boundary conditions, the complete aircraft was suspended from a crane. A spring was placed between the crane and a stiff strap used to hold the aircraft, as shown in Fig. 7, allowing a quasi-free support condition while maintaining overall system stability. The aircraft was tested in full flight configuration, including all batteries, onboard systems, and instrumentation, to ensure representative mass and inertia properties.


Figure 7: GVT of the full aircraft configuration.

The spring was selected to provide a low vertical bouncing frequency of approximately 1 Hz, while remaining within its linear operating range. This choice ensures sufficient separation from the first bending mode of the wing, thereby reducing potential coupling between the suspension dynamics and the structural modes of interest. As a result, the influence of the support system on the identified modal properties is minimized, improving the accuracy and reliability of the structural dynamics identification.

## 5 SIMULATION TESTING ENVIRONMENT BASED ON MODSIG

A Simulation Testing Environment (STE) was developed to support the design and preparation of the flight test campaign. The framework is implemented in MATLAB/Simulink using ModSiG as the flight dynamics solver and is coupled with X-Plane for real-time visualization [16–18]. The general structure of the STE is shown in Fig. 8. The environment allows the use of both automatic inputs (e.g., steps, doublets, and frequency sweeps) and manual inputs through a joystick or the actual radio controller, enabling consistent maneuver definition as well as pilot-in-the-loop simulations.

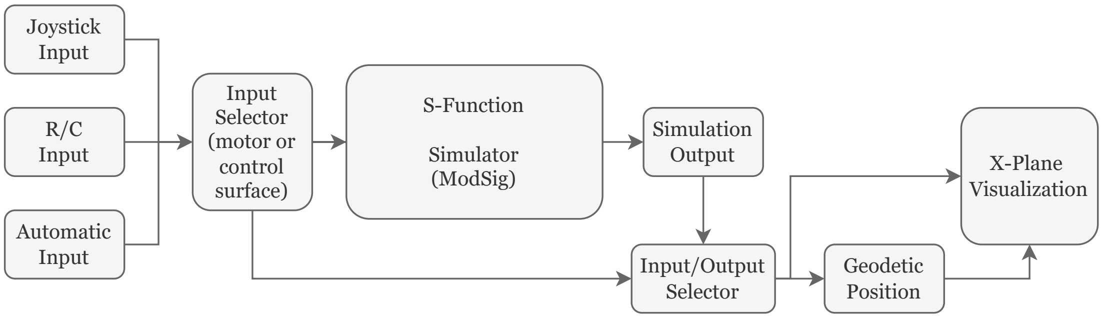


Figure 8: Simulation testing environment for flight test design

The STE supports different control architectures and levels of model fidelity, including quasi-steady and unsteady aerodynamics with coupled linear structural dynamics. For this work, a real-time-capable flexible aircraft model of the TU-Flex-FW configuration is employed [11]. The simulation outputs are processed and transmitted to X-Plane via UDP, allowing visualization of the aircraft motion, control surface deflections, and flight states. The corresponding animated model is presented in Fig. 9. Although structural deformation is computed within the model, it is not visualized to ensure real-time performance.

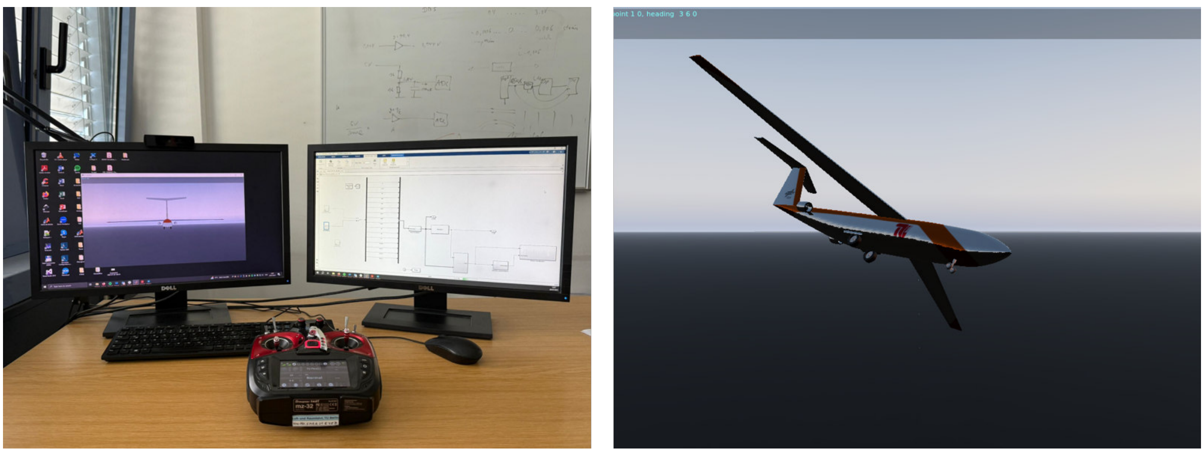

Figure 9: STE direct flight setup and animation

The environment also incorporates multiple control logics, including manual control through a direct connection with the actual radio controller, as shown in Fig. 9, predefined maneuver inputs, and closed-loop control configurations. Predefined maneuvers enable repeatable excitation of the aircraft dynamics, supporting system identification and model validation [19, 20]. Additionally, stability augmentation and higher-level control strategies can be implemented and evaluated within the same framework. This allows progressive testing of control concepts and a safe transition between control modes.

Overall, the STE enables the evaluation of flight test maneuvers, supports model validation, and provides a platform for pilot training. It ensures that all planned experiments can be assessed and refined in a controlled environment prior to flight testing, reducing risk and improving the design of the experimental campaign.

## 6 GROUND TESTS

The objective of this phase is to verify the full system functionality and ensure pilot confidence prior to flight testing. This campaign combines a series of ground-based evaluations with progressive taxi tests to assess the readiness of the aircraft. Initial tests focus on electromagnetic compatibility, communication integrity, and control system functionality, including telemetry bandwidth adjustment, link range verification, and link loss behavior. Flight control checks are performed to ensure full and free movement of all control surfaces, together with engine response and symmetry verification. In parallel, electrical and avionics systems are evaluated through voltage measurements, sensor calibration, and validation of data acquisition and telemetry transmission, including the structural dynamics measurement system. Indications and onboard displays are cross-checked with ground station data, and weight and balance are verified to ensure that the aircraft operates within allowable limits.

Following these checks, low-speed taxi tests are conducted up to 40% of the take-off velocity to evaluate ground maneuverability, steering response, braking performance, and communication link stability. Once satisfactory performance is achieved, high-speed taxi tests up to 80% of the take-off velocity are performed to assess aircraft behavior under increased dynamic loads, including directional stability, control effectiveness, and data integrity. Throughout all tests, communication latency, telemetry performance, and sensor availability are continuously monitored. The completion of this phase is defined by the absence of critical anomalies, stable system performance, and pilot confirmation of safe and predictable handling, enabling progression to the flight test campaign.

## 7 RESULTS

This section presents the results obtained following the bottom-up approach defined for the TU-Flex, including the characterization of the mass and inertia properties, the identification of the structural dynamics through the full-aircraft GVT, and the evaluation of system performance during the taxi test campaigns. The section also summarizes the flight test maneuvers selected for the initial campaign and reports preliminary observations from the first flight test.

### 7.1 CG and Inertia Measurements

The average take-off weight of the TU-Flex-FW is 23.25 kg. The CG of the aircraft is located on $0.22\bar{c}$, 7 mm to the right of the fuselage's center line and 50 mm below the wings' leading edge line. This longitudinal position ensures positive static stability of 15% while maintaining a reasonable balance between pitch stiffness and trim drag. The small lateral offset is attributed to minor component asymmetries and is negligible for flight performance, as it can be compensated using control surfaces. The vertical CG position contributes to stabilizing pendulum effects but may also influence lateral–directional coupling.

The resulting averaged inertia values for the TU-Flex FW are $I_{xx} = 4.6$, $I_{yy} = 5.68$ and $I_{zz} = 11.69$ kg $m^2$. These results are compared with the most recent CAD-based estimates, which yield $I_{xx} = 3.36$, $I_{yy} = 7.78$ and $I_{zz} = 10.56$ kg $m^2$. This corresponds to deviations of $+37\%$ for $I_{xx}$, $-27\%$ for $I_{yy}$, and $+11\%$ for $I_{zz}$. While the values remain consistent in order of magnitude, the discrepancies highlight the limitations of relying solely on CAD-based inertia estimations, which are sensitive to modelling assumptions, component simplifications, and uncertainties in the actual mass distribution. In particular, the CAD model does not fully capture the exact placement and distribution of cabling, sensors, adhesive materials, screws, bolts, and other fixation components as implemented in the manufactured aircraft. Although these elements may individually contribute small masses, their combined effect and spatial distribution can significantly influence the overall inertia properties. The experimental determination is therefore essential to obtain reliable inertia data for flight dynamics analysis and to account for the differences between the idealized CAD representation and the physical aircraft configuration.

### 7.2 Full Aircraft Ground Vibration Testing

The GVT was performed to identify the frequencies and mode shapes of the full aircraft configuration and to assess the influence of the fuselage connection on the natural frequencies of the wings. A summary of the first seven identified modes is given in Table 1, including their description, frequency, and MAC values with respect to the FEM modal shapes. The full MAC matrix is presented in Fig. 10, while the comparison between FEM and GVT mode shapes is shown in Fig. 11.

Table 1: Identified structural modes and comparison between FEM and GVT MAC.

| Mode | Description | $f$, Hz | MAC FEM/GVT |
|---|---|---|---|
| 1 | First bending | 5.55 | 0.99 |
| 2 | First asymmetric with tail component in phase with the left wing | 10.27 | 0.91 |
| 3 | First asymmetric with tail component in phase with the right wing | 15.98 | 0.94 |
| 4 | Second bending | 21.21 | 0.98 |
| 5 | Coupled stabilizer mode 1 | 22.60 | 0.77 |
| 6 | Coupled stabilizer mode 2 | 27.17 | 0.75 |
| 7 | First in-plane mode | 33.30 | 0.97 |

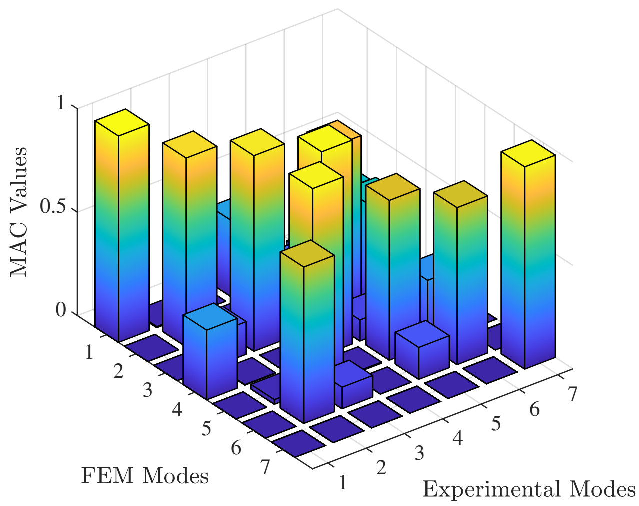


Figure 10: Full aircraft FEM/GVT MAC.

The identified modal characteristics show a consistent structural behavior of the full aircraft. The first mode corresponds to the global first bending at 5.55 Hz, followed by two asymmetric modes at 10.27 Hz and 15.98 Hz, where the tail component is in phase with the left and right wing, respectively. The second bending mode is identified at 21.21 Hz, while modes five and six correspond to coupled stabilizer modes at 22.60 Hz and 27.17 Hz, showing a strong contribution of the tail and fuselage. The seventh mode represents the first in-plane deformation at 33.30 Hz.

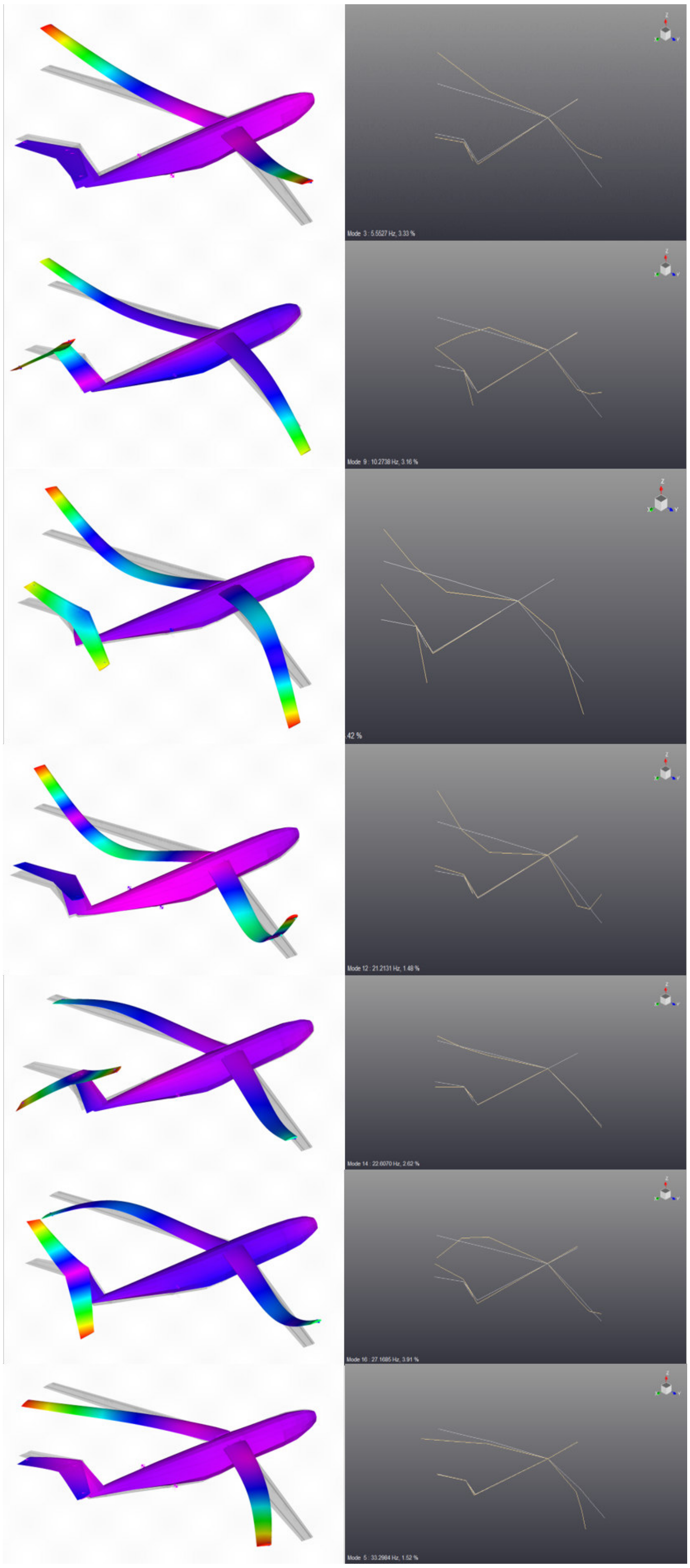

Figure 11: Comparison between the identified aircraft mode shapes and the FEM.

The comparison between FEM and GVT results demonstrates an overall very good agreement. The global bending modes are captured with excellent accuracy, as reflected by MAC values of 0.99 and 0.98 for the first and second bending modes, respectively. The asymmetric modes (modes 2 and 3) as well as the first in-plane mode (mode 7) also show strong correlation, with MAC values above 0.9, indicating a consistent representation of both symmetric and asymmetric deformation patterns.

Lower MAC values are observed for the coupled stabilizer modes (modes 5 and 6), with values of 0.77 and 0.75. These discrepancies are attributed to the strong influence of wing–tail interaction, which is more sensitive to modeling assumptions and sensor placement. In particular, the current sensor distribution does not fully capture the detailed tail dynamics required for an accurate modal correlation. An increased sensor density in the tail region or an optimized sensor layout would likely improve the agreement. Future works will include this consideration in the next GVT campaign. Nevertheless, the qualitative similarity between experimental and numerical mode shapes remains well preserved, and the correlation is considered acceptable at this stage.

A comparison with the wing-only GVT highlights the influence of the fuselage connection. The first bending mode increases from 5.297 Hz to 5.55 Hz (approximately 4.8%), while the second bending mode shifts from 20.160 Hz to 21.21 Hz (approximately 5.2%). Similarly, the first in-plane mode increases from 32.269 Hz to 33.30 Hz (approximately 3.2%). These shifts indicate an increase in global stiffness due to the fuselage integration.

The actual wing/fuselage connection is not yet modelled in full detail in the FEM. Instead, the integration between the wing and fuselage is represented using RBE3 elements, which distribute the connection loads from the wing attachment points to multiple nodes on the fuselage floor and skin. Therefore, the observed frequency shifts mainly reflect the stiffness contribution introduced by this simplified structural coupling. The remaining modes are not directly comparable, as they are primarily driven by the dynamics of the tail and fuselage.

### 7.3 Flight-Test Maneuver Set for Model Identification

The TU-Flex model implemented in ModSig was updated using the complete set of previously obtained experimental results. In its current form, the model incorporates the measured mass properties, including weight and inertias, as well as the experimentally identified natural frequencies based on validated mode shapes. In addition, the aeroelastic representation of the wing has been refined using results from the wind tunnel test campaign [13]. This updated model serves as the basis for the definition of the flight-test excitation maneuvers presented in this subsection.

Based on the aeroelastic and flight dynamics analyses, a set of excitation maneuvers was defined to support the identification and tuning of the aircraft model. All selected inputs satisfy the structural constraints of the TU-Flex wind tunnel wing test, namely a maximum strain limit of 6000 $\mu\varepsilon$ and a maximum vertical wing-tip displacement of 12% [6]. The resulting maneuver set represents a compromise between sufficient modal excitation and structural safety.

The longitudinal dynamics are primarily excited using elevator-based inputs. The short-period mode is targeted through a pitch doublet at 1.59 Hz. To ensure excitation of the first wing bending mode and its interaction with rigid-body motion, additional doublets at approximately 5 Hz are applied using both elevators and symmetric outer ailerons. Chirp inputs spanning 0.5–8 Hz further enable simultaneous identification of rigid-body and structural modes.

Lateral-directional dynamics are addressed through rudder and aileron inputs. The Dutch roll mode is excited using a rudder doublet at 0.65 Hz, while roll dynamics are identified through step or 3-2-1-1 aileron inputs. The spiral mode is evaluated using a rudder 2-1-1 input, allowing the low-frequency mode to develop naturally. Finally, asymmetric structural modes are excited by higher-frequency chirps applied to the rudder and outer ailerons, covering the relevant structural bandwidth.

The complete set of excitation maneuvers is summarized in Table 2. These inputs provide sufficient excitation of both rigid-body and aeroelastic modes while remaining within the operational and structural limits of the aircraft, at the cruise speed of 30 m/s. As such, they define the baseline flight-test campaign for model identification and subsequent control development.

Table 2: Summary of control inputs for excitation of flight dynamics and structural modes.

| Mode | Control Surface | Input Type | Frequency / Duration | Amplitude |
|---|---|---|---|---|
| Short-Period | Elevators | Doublet | 1.59 Hz | 5° |
| Short-Period | Elevators | Chirp | 0.5–8 Hz in 10 s | 5° |
| Struct. Bend. (long.) | Elevators | Doublet | ∼5 Hz | 5–10° |
| Struct. Bend. (long.) | Outer Ailerons (sym.) | Doublet | ∼5 Hz | 5–10° |
| Struct. Modes (long.) | Elevators & Outer Ailerons (sym.) | Chirp | 0.5–8 Hz in 10 s | 5° |
| Dutch Roll | Rudder | Doublet | 0.65 Hz | 5° |
| Roll Mode | Inner to Outer Ailerons | Step or 3-2-1-1 | 2 Hz | 5° |
| Spiral Mode | Rudder | 2-1-1 | – | ∼10° bank |
| Struct. Modes (lat.) | Rudder | Chirp | 0.5–10 Hz in 8 s | 5° |
| Struct. Modes (lat.) | Outer Ailerons (asym.) | Chirp | 2–13 Hz in 8 s | 5° |

### 7.4 Ground Tests

The TU-Flex test campaign occurred at the Heilbad Heiligenstadt Airfield in Lower Saxony, Germany. The focus of the first set of tests was to evaluate electromagnetic interference, communication, and control link stability. The aircraft was placed at the center of the runway and then, using its own propulsion system, displaced to the extremes of the 700 m track.

It is important to point out that the first configuration of the aircraft used a 2.4 GHz signal for both the telemetry system and the radio receiver. At approximately 60 m, the telemetry signal increased in strength; however, the link between the radio controller and the receiver was lost. The telemetry system used in the aircraft is a SkyHopper PRO system, which allows adjustment of the transmission bandwidth limits.

To avoid interference with the receiver, the telemetry system frequency was reduced to 2.3 GHz. At the same time, and to introduce redundancy, the original radio controller and receiver were replaced with a FrSky Tandem X18R system. This controller allows connection to two receivers on the aircraft for redundancy and operates in both 2.4 GHz and 868 MHz bands. Consequently, six antennas were installed on the aircraft, four for the 2.4 GHz and two for the 868 MHz.

To evaluate possible shadowing of the control link signal caused by the carbon fiber fuselage, a test was performed in which the aircraft was rotated 360 degrees with respect to the radio controller and the ground station. This allowed assessment of the influence of aircraft orientation on signal quality. It was observed that when the carbon fiber tail was pointing toward the ground station, there were cases of signal loss in either the telemetry system or the receiver.

Therefore, both antennas were relocated outside the aircraft, on the upper and lower sections of the fuselage, as shown in Fig. 2. This antenna configuration maintained a continuous connection with both the receiver and the ground station throughout the ground test campaign. The aircraft was able to be displaced over a distance exceeding one kilometer without link loss, and the influence of aircraft orientation on signal quality was eliminated.

The second set of ground tests consisted of ground maneuverability runs. The pilot's task was to perform precision maneuvers on the runway to assess the aircraft's controllability on the ground. For this purpose, an oval pattern was completed along the runway, following the centerline, performing 180° turns, and returning to the centerline. After tuning the nose landing gear orientation, the pilot reported good handling qualities during slow taxi maneuvers.

The next phase included acceleration runs to train the pilot and gain experience with the evolution of handling qualities as dynamic pressure increases. The first runs reached 40% of the stall speed, followed by runs up to 80%. During these tests, the pilot reported increased rudder control authority. The symmetry of the propulsion system was also evaluated, with no noticeable influence on the aircraft's directional behavior. Once the nose landing gear was properly trimmed, the aircraft could be kept aligned with the runway centerline. Figure 12 shows a picture of the aircraft during these procedures. The pilot was satisfied with the aircraft's performance and controllability on the ground, as well as with the available propulsion power. Throughout these tests, the telemetry and control link remained stable, and more than 150 measurement outputs were successfully recorded and transmitted to the ground station.

Figure 12: Ground maneuverability runs.

### 7.5 Observations from the First Flight Test

The first flight test demonstrated that the aircraft is capable of safe takeoff and flight operation. The vehicle showed stable and controllable behavior throughout the flight. The data link remained stable during the entire test, and the main aircraft signals were successfully transmitted to the ground station, allowing real-time monitoring of the system.

Structural deformation was clearly observed during flight, with initial estimates remaining within the predicted levels obtained from the modeled load cases. This confirms that the aeroelastic behavior of the aircraft is consistent with the expected response of the flexible configuration.

Figure 13 shows 15 s of the first flight, which includes the acceleration run, the takeoff, and the climb up to 40 m. In terms of performance, the aircraft took off at approximately 1.2 times the stall speed, corresponding to 21.25 m/s. After applying 100% motor command, takeoff was achieved in 9.427 s, requiring a ground roll of 66 m. During flight, the aircraft operated within a speed range from 1.2 times the stall speed up to 45 m/s. A maximum climb rate of 2.3 m/s was observed at an airspeed of 36 m/s. This flight test also showed that the selected propulsion system is sufficient to power the aircraft along the entire flight envelope.

The maximum angle of attack achieved during takeoff was approximately 4.5 deg after the initial pitch rate of around 5 deg/s. The maximum load factor during this takeoff phase was 1.6 g, whose effect is also observable in the structure. In the strain plot, it is possible to observe the increase in strain due to the deformation of the wing under aerodynamic loading. The oscillation of the wing was also monitored by the three IMUs installed in the structure; in the plot, the dynamics of the right external IMU are presented. The control surface deflections show the level of controllability of the aircraft: a command of approximately -3 deg in the elevator gave the pilot enough authority to rotate the aircraft. The aileron and rudder were activated during this maneuver to compensate for lateral winds at the moment of the run, and a permanent -3 deg rudder deflection was added during the taxiing runs to provide lateral trim.

To evaluate the validity of the TU-Flex design framework, a comparison is performed between the flight test data and the flexible flight dynamics model ModSiG-FMRA [11] used during the aircraft design process. It is important to point out that this model only includes the structural dynamics, inertia, and mass property updates resulting from the full-aircraft ground tests, as well as the lift distributions tuned from the wind tunnel tests. The flight dynamics model has not yet been tuned.

Figure 14 shows a 17 s comparison between the acquired flight data and the untuned flight dynamics model. In this Fig., the velocity ($V$), the angle of attack($\alpha$), the pitch rate ($q$), the pitch angle ($\theta$), the roll rate ($p$), the roll angle ($\phi$), the yaw rate ($r$), the control surfaces deflection ($\delta_e$, $\delta_{aer}$), the CG load factor ($\eta_z$) and the estimated/modeled vertical right wingtip displacement are presented ($\delta_z$). The model is trimmed at the same operating point as the aircraft and is fed with the measured control inputs. At first glance, the comparison shows that the design model is capable of capturing the main trends in the evolution of the primary rigid-body flight dynamics states. There is particularly good agreement on the longitudinal axis, where both the magnitudes and frequencies observed in the pitch rate and pitch angle are matched. The biggest mismatch on this axis is observed in the velocity estimation. In this case, the overall trend is captured; nevertheless, the flight dynamics model seems to underestimate the observed increase in speed. This behavior could be attributed to an overestimation of the drag in the model.

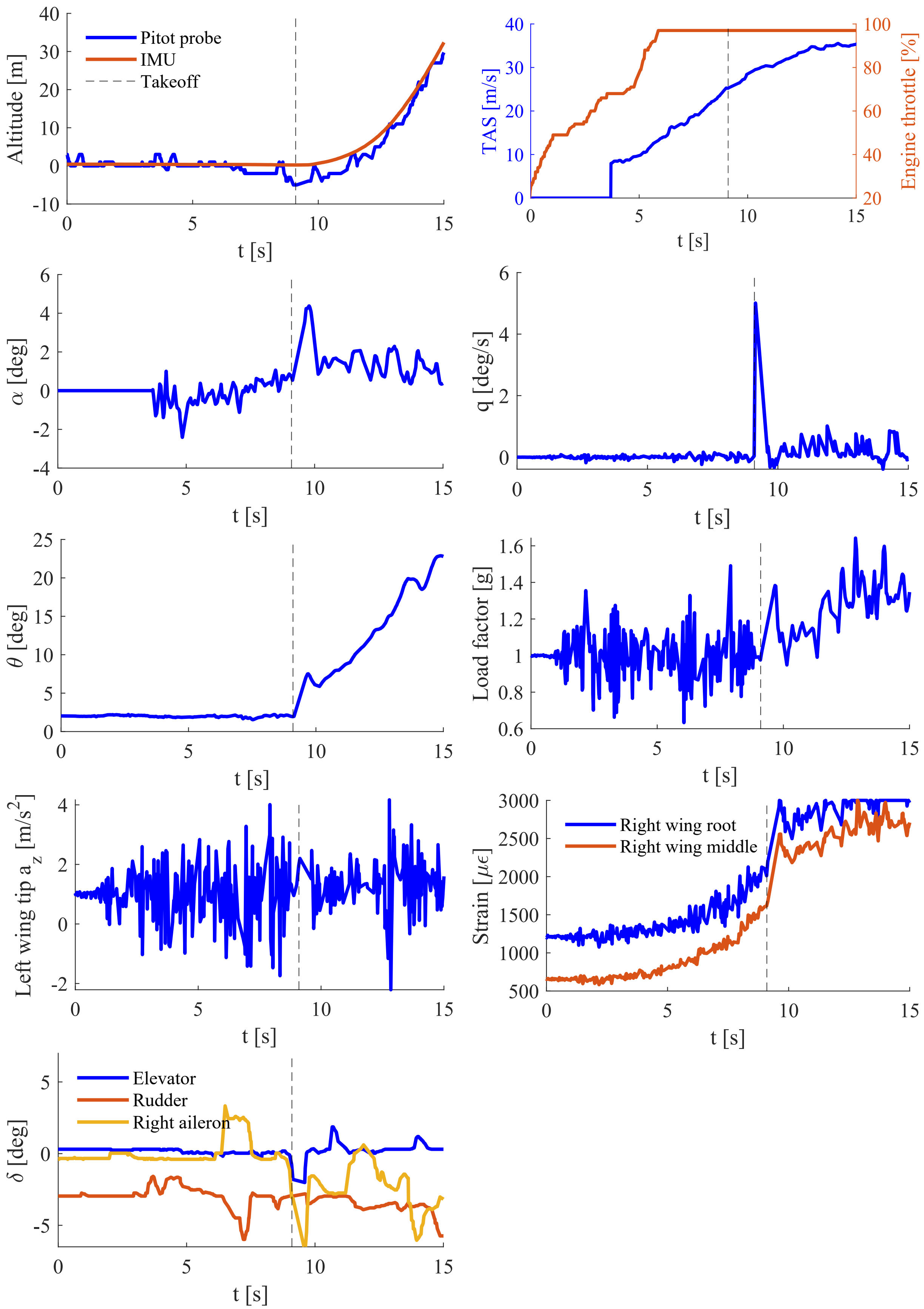


Figure 13: TU-Flex take off sensor outputs.

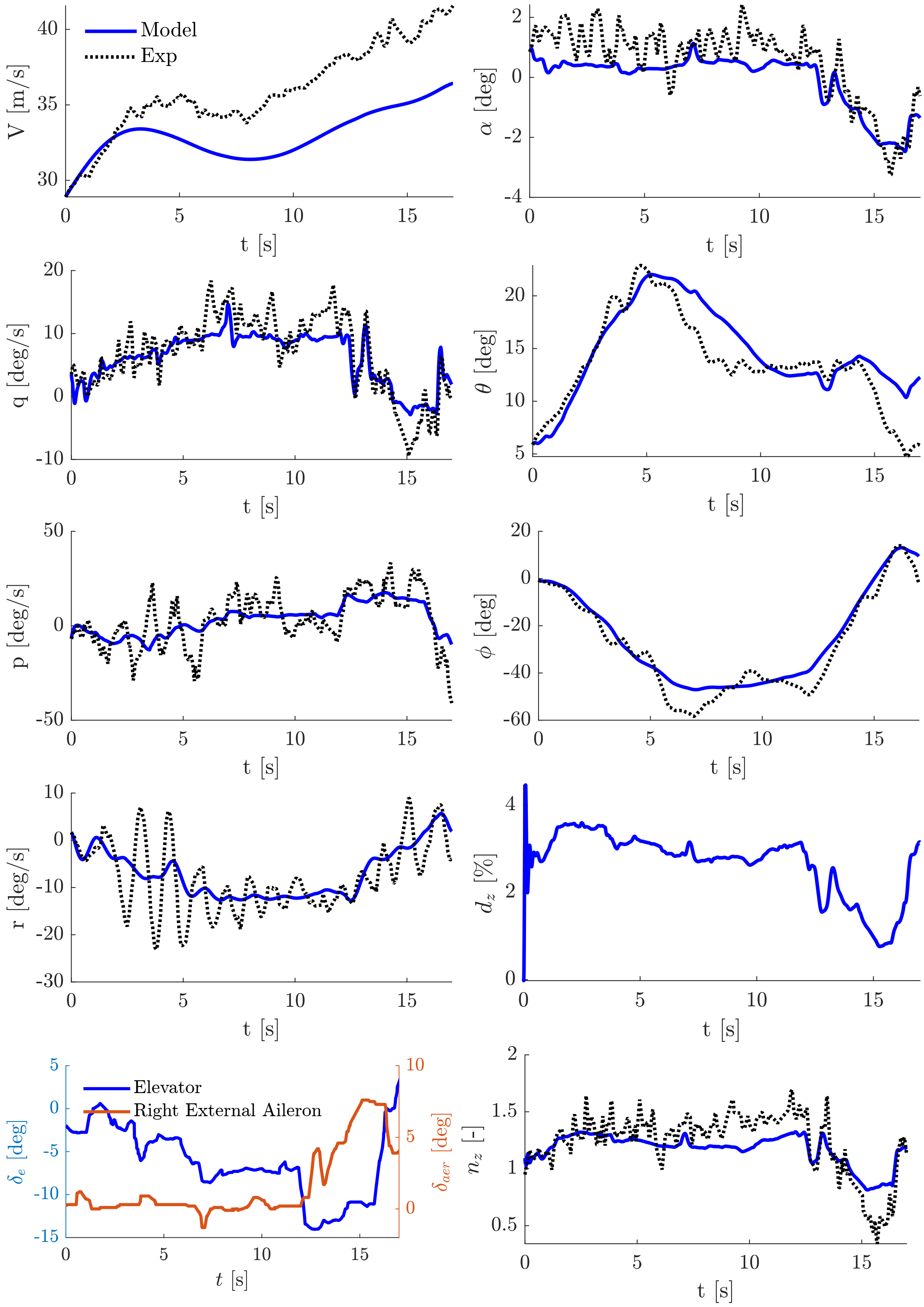


Figure 14: Flight test data and untuned flight dynamics model comparison.

The excursions of the yaw rate and roll rate associated with the Dutch roll are larger than anticipated, and curiously, the yaw rate excursions appear less damped than expected. It is also important to point out that the aerodynamic model neglects the influence of the fuselage. Nevertheless, the mean trends are still captured by the model, and there is good agreement with the roll angle.

The presented results do not correspond to a dedicated control input maneuver, but rather to open-loop flight conditions. In Fig. 14, it is possible to observe the variation of the control surface commands, where no isolated input is applied, but instead a combination of elevator and aileron commands. This further highlights the capability of the proposed design framework to predict the main trends of a flying flexible aircraft even under complex combined excitations.

Figures 15 and 16 show impressions from the first flight test. In Fig 15, it is possible to observe the aircraft during the flight test entering straight flight condition and at the beginning of a turn. Figure 16 (left) highlights the level of structural deformation reachable by the aircraft. In this condition, the aircraft was flying at 45 m/s under a load factor of 2.3 g, resulting in a wingtip vertical displacement of approximately 0.28 m, corresponding to about 16% of the semi-span. The FEM model of the aircraft was loaded in NASTRAN using these flight conditions as input and subsequently overlaid on the picture (Fig. 16 (right)). In this first comparison, a good agreement between the model and the image can be observed. Future flights will allow the collection of additional data to perform a more detailed comparison.

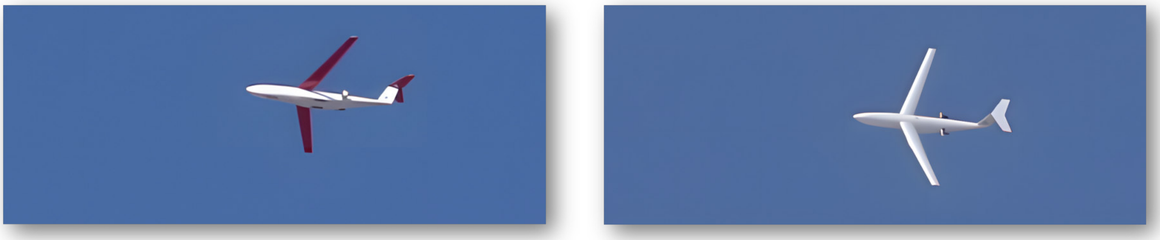

Figure 15: TU-Flex during the first flight test.

Figure 16: TU-Flex maximum in-flight load case: image (left) vs. FEM result (right).

Overall, the results from the first flight test indicate that the demonstrator is capable of operating as a flexible aircraft, with behavior consistent with the expected aeroelastic characteristics.

## 8 SUMMARY AND CONCLUSIONS

This work presents the definition, implementation, and experimental validation of a structured, bottom-up approach for airworthiness assessment and flight-test preparation of a flexible aircraft demonstrator. Rather than addressing the complete aircraft design process, the focus is placed on the expansion of the experimental validation block within the TU-Flex workflow. This block provides the necessary experimental feedback to update the structural, aeroelastic, inertial, and flight dynamics models before progressing toward flight testing.

The proposed approach connects component-level validation with full-aircraft evaluation. Starting from previous wing-level static, dynamic, and aeroelastic tests, the methodology is extended to the complete aircraft through center of gravity and inertia measurements, full-aircraft ground vibration testing, system integration checks, and ground maneuverability evaluations. These tests allow the identification of relevant aircraft properties and the verification of the platform readiness under controlled conditions.

The measured mass and inertia properties highlighted the importance of experimental characterization, since noticeable differences were observed with respect to the CAD-based estimates. The full-aircraft GVT showed good agreement between experimental and numerical mode shapes, particularly for the main bending and in-plane modes. These results provide updated information for the flexible aircraft model and support the preparation of the flight-test campaign.

The simulation testing environment was used to evaluate the aircraft response and define a set of flight-test maneuvers for model identification. Together with the ground test campaign, this enabled a progressive reduction of risk before the first flight. The ground tests confirmed adequate communication link stability, system functionality, controllability on the ground, and propulsion performance.

The first flight test demonstrated that the aircraft is capable of safe takeoff and stable operation, while maintaining reliable data transmission to the ground station. Structural deformation was clearly observed during flight and remained within the expected range for the modeled load cases.

Overall, the results show that the expanded experimental validation block provides an effective connection between ground testing, model updating, simulation, and flight-test preparation. The TU-Flex demonstrator is therefore able to operate as a flexible aircraft platform and to represent the coupled structural and flight dynamics required for future model validation and control development activities.

## ACKNOWLEDGEMENTS

This study was financed in part by the German Federal Ministry for Economic Affairs and Climate Action (BMWK) due to a resolution of the German Federal Parliament within the scope of the LuFo VI-1 project FlexFuture (Grant number 20E2120A).

## 9 REFERENCES

[1] Palacios, R. and Cesnik, C. E. S. (2023). *Dynamics of Flexible Aircraft*. Cambridge University Press. doi:https://doi.org/10.1017/9781108354868.

[2] González, P. (2026). *High-Aspect-Ratio-Wing Aircraft Flying Demonstrator: Design, Construction and Testing Study Case: TU-Flex*. Habilitation, Technische Universität Berlin, Berlin.

[3] González, P. J., Stavorinus, G., Silvestre, F. J., et al. (2023). Tu-flex: A very-flexible flying demonstrator with a generic transport aircraft configuration. In *AIAA SCITECH 2023 Forum*. doi:10.2514/6.2023-1312.

[4] González, P. J., Shahi, H., Meddaikar, M. Y., et al. (2022). Flexible-wing design process for tu-flex demonstrator. In *19th International Forum on Aeroelasticity and Structural Dynamics, IFASD 2022*.

[5] González, P., Stavorinus, G., Shahi, H., et al. (2022). A structural preliminary design of a flexible flying demonstrator. In *Proceedings*. 33rd Congress of the International Council of the Aeronautical Sciences - ICAS 2022At:, Stockholm, Sweden: ICAS. ISBN 978-171387116-3.

[6] González, P. J., Barbosa, G. C., Quesada, A. A., et al. (2024). Wind tunnel testing and modal validation of tu-flex's high aspect-ratio wings. In *IFASD 2024 - International Forum on Aeroelasticity and Structural Dynamics,*.

[7] Voß, A. (2020). Loads kernel user guide. Tech. Rep. DLR-IB-AE-GO-2020-136, German Aerospace Center (DLR). Https://elib.dlr.de/140268/.

[8] Voß, A. (2020). *Design and structural optimization of a flying wing of low aspect ratio based on flight loads*. Doctoral thesis, Technische Universität Berlin, Berlin. doi:10.14279/depositonce-9858.

[9] Waszak, M. R. and Schmidt, D. K. (1988). Flight dynamics of aeroelastic vehicles. *Journal of Aircraft*, 25(6), 563–571. doi:https://doi.org/10.2514/3.45623.

[10] Silvestre, F. J. and Luckner, R. (2015). Experimental validation of a flight simulation model for slightly flexible aircraft. *AIAA Journal*, 53(12), 3620–3636. doi:10.2514/1.J054023.

[11] Quesada, A. A. G., González, P. J., Barbosa, G. C., et al. (2024). Influence of nonlinear aerodynamic effects on high aspect ratio aircraft model. In *IFASD 2024 - International Forum on Aeroelasticity and Structural Dynamics,*.

[12] SSR, F. (2025). pytlo: Tapered composite laminate optimization via genetic algorithm. `https://gitlab.com/FGS_SSR/pytlo`.

[13] Stavorinus, G., González, P. J., Barbosa, G. C., et al. (2026). Aeroelastic model update for a flexible wing using experimental data. In *IFASD 2026 - International Forum on Aeroelasticity and Structural Dynamics,*.

[14] Soule, H. A. and Miller, M. P. (1934). The experimental determination of the moments of inertia of airplanes. *NASA*, TR(467).

[15] Miller, M. (1930). An accurate method of measuring the moments of inertia of airplanes. Tech. rep., Langley Memorial Aeronautical Laboratory.

[16] González, P., Boschetti, P., Cárdenas, E., et al. (2010). Evaluation of the flying qualities of a half-scale unmanned airplane via flight simulation. In *48th AIAA Aerospace Sciences Meeting Including the New Horizons Forum and Aerospace Exposition*. p. 298. doi:https://doi.org/10.2514/6.2010-298.

[17] Eltaher, Z. (2024). *Modelling and implementation of a real-time flexible aircraft simulation environment with animation of flight path, attitude and airframe deformation*. Master's thesis, Technische Universität Berlin, Berlin.

[18] Sjafii, D. (2025). *Development of a flight dynamic model for an unmanned remotely piloted aircraft*. Bachelor's thesis, Technische Universität Berlin, Berlin.

[19] González, P. J., Cesnik, C. E. S., and Silvestre, F. J. (2018). Implementation and flight testing of an enhanced stability system for a very flexible aircraft. In *Proceedings*, ICAS 2018-0534. 31st Congress of the International Council of the Aeronautical Sciences, Belo Horizonte - MG - Brazil: ICAS.

[20] Guimarães Neto, A. B., Barbosa, G. C., Paulino, J. A., et al. (2023). Flexible aircraft simulation validation with flight test data. *AIAA Journal*, 61(1), 285–304. doi:https://doi.org/10.2514/1.J060960.

**COPYRIGHT STATEMENT**